

Bone Matrix Composition Following PTH Treatment is Not Dependent on Sclerostin Status

Ryan D. Ross¹ · Maleeha Mashiatulla^{1,2} · Alexander G. Robling^{4,5} ·
Lisa M. Miller^{6,7} · D. Rick Sumner^{1,2,3}

Received: 18 September 2015 / Accepted: 9 October 2015 / Published online: 29 October 2015
© Springer Science+Business Media New York 2015

Abstract Sclerostin and parathyroid hormones are strong negative and positive regulators of bone formation, respectively. The anabolic response induced by intermittent (iPTH) treatment is sclerostin status-dependent. However, the interaction between sclerostin and iPTH at the matrix level is unknown. The goal of the current study was to determine if iPTH treatment affects matrix composition and, if so, whether these effects are dependent on sclerostin status. Humeral trabecular and cortical bone sites from 16 week old male wild-type (WT) and sclerostin knockout (KO) mice, which had been treated with vehicle or iPTH from age 10–16 weeks, were examined by micro-computed tomography (μ CT) to measure bone volume, backscatter scanning electron microscopy (bSEM) to assess global mineralization,

and Fourier transform infrared microspectroscopy (FTIRM) to examine matrix composition (mineral-to-matrix ratio, crystallinity, collagen cross-link ratio, and carbonate substitution). The FTIRM measurements were restricted to the tissue formed during the 6-week treatment period. iPTH treatment led to increased trabecular bone volume ($p < 0.001$) and this effect was much greater in KO mice than WT mice (interaction effect, $p < 0.001$). iPTH treatment led to reduced trabecular crystallinity ($p = 0.047$), increased cortical bone area ($p < 0.001$), decreased cortical bone crystallinity ($p = 0.002$) and increased cortical bone collagen cross-linking ($p = 0.028$) to similar degrees in both WT and KO mice. Compared to WT mice, sclerostin KO mice had higher trabecular and cortical bone mass ($p < 0.001$) and lower mineral-to-matrix ratio in the trabecular ($p = 0.010$) and cortical ($p = 0.016$) compartments. Thus, iPTH-induced changes in bone mass are dependent upon sclerostin status in the trabecular compartment, but not in the cortical compartment. In contrast, iPTH-induced changes in matrix composition are sclerostin-independent in both trabecular and cortical compartments.

✉ Ryan D. Ross
ryan_ross@rush.edu

D. Rick Sumner
Rick_Sumner@rush.edu

¹ Department of Anatomy and Cell Biology, Rush University Medical Center, 600 South Paulina, Suite 507, Chicago, IL 60612, USA

² Department of Bioengineering, University of Illinois Chicago, Chicago, IL, USA

³ Department of Orthopaedic Surgery, Rush University Medical Center, Chicago, IL, USA

⁴ Department of Anatomy and Cell Biology, Indiana University, Indianapolis, IN, USA

⁵ Richard L. Roudebush VA Medical Center, Indianapolis, IN, USA

⁶ Department of Biomedical Engineering, Stony Brook University, Stony Brook, NY, USA

⁷ National Synchrotron Light Source-II, Brookhaven National Laboratory, Upton, NY, USA

Keywords Mineralization · Bone quality · Matrix composition · Sclerostin · Parathyroid hormone

Introduction

Pharmacological control of the bone formation process presents an opportunity to treat low bone mass conditions such as osteoporosis. Currently, there is only one clinically approved anabolic, or bone forming agent—a 34-residue fragment of the human parathyroid hormone (PTH). PTH directly activates osteoblasts and indirectly activates osteoclasts, subsequently up regulating the bone

remodeling process [7, 17]. If given intermittently at low dose, PTH increases bone mass by preferentially upregulating bone formation over resorption [10]. Additional anabolic agents currently in development include sclerostin antibody. Sclerostin, encoded by the *SOST* gene, is a soluble antagonist to the Wnt co-receptors Lrp5/6 that limits bone formation by inhibiting osteoblast differentiation, activity, and upregulating apoptosis [33]. Neutralizing monoclonal antibodies to sclerostin increase bone formation rates and bone mass in rodents and non-human primates, and several are currently in phase II/III clinical trials [23–25, 28]. Emerging evidence has suggested that the anabolic responses associated with PTH treatment and sclerostin suppression are not independent. Indeed, treatment with PTH has been shown to cause substantial sclerostin suppression [3, 11] and the anabolic effects of PTH appear to depend on sclerostin status [14, 29].

Bone quality describes the factors, independent of bone mineral density, that determine bone strength and fracture risk [8]. These factors range in scale from the structural organization of bone to the nanoscale matrix composition. At the nanoscale, bone matrix is composed primarily of organic type I collagen and inorganic hydroxyapatite mineral crystals. Alterations to either phase can have detrimental consequences on the strength of bone [5].

There has been growing interest in the quality of bone formed during treatment with bone-targeted therapies. In the case of PTH, previous studies have found that treatment of animals and humans with PTH generally triggers a slight reduction in the average tissue mineralization and an increase in the mineralization heterogeneity [6, 12, 19, 20, 26, 27]. In contrast, suppression of sclerostin with sclerostin antibody does not impact global tissue mineralization in nonhuman primates or rats [31]. It is unclear whether the mineralization differences between PTH and sclerostin inhibition are caused by differences in the model systems used or if there are differential effects of PTH and sclerostin suppression on the matrix maturation process. The goals of the present study were to compare the effects of PTH treatment and sclerostin deficiency on bone matrix composition in a single model system and to determine if PTH-induced matrix effects were dependent on sclerostin status.

Materials and Methods

Mouse Tissues

Sclerostin intact wild-type (WT) and sclerostin knockout (*SOST* KO) male mice bred on a mixed 129/SvJ and Black Swiss genetic background were obtained from a previously published study [29]. The development of the mice was

previously described in detail [16]. Injections of 100 μ L of either vehicle or 90 μ g/kg intermittent parathyroid hormone (iPTH) were given daily for 7 days per week between 10 and 16 weeks of age. Fluorochrome labels were injected subcutaneously 3 days before the first PTH injection (oxytetracycline) and 3 days before sacrifice (alizarin complexone). Therefore, the labels differentiated the tissue that was formed during the 6-week treatment period from tissue formed prior.

A total of 24 animals were split between four groups; (1) WT treated with vehicle ($n = 6$), (2) WT treated with PTH ($n = 6$), (3) *SOST* KO treated with vehicle ($n = 6$), and (4) *SOST* KO treated with PTH ($n = 6$). To measure bone matrix composition, the right humeri were fixed in 70 % ethanol and all subsequent analyses were performed on the trabecular and cortical bone.

Micro-computed Tomography (μ CT)

Humeri were scanned submerged in 70 % ethanol perpendicular to the bone's long-axis using 55 kVp and 145 μ A, with a 300 ms integration time and a 10 μ m isotropic voxel size (Scanco μ CT 40). Trabecular bone architecture was measured in a proximal region just distal to the growth plate through 30 % of the total length. Primary trabecular parameters included bone volume per total volume (BV/TV), trabecular number, trabecular thickness, and trabecular spacing. Cortical geometry was measured in a 100 slice diaphyseal region located just distal to the deltoid tuberosity at 55 % of the total length of the humerus. Primary cortical parameters included cortical area, total area, medullary area, and cortical thickness. All parameters are reported using conventional nomenclature [4].

Section Preparation

Following μ CT scanning, bones were dehydrated in a graded series of ethanol solutions and embedded in a non-infiltrating epoxy resin (EpoThin, Buehler). A series of 700 μ m thick transverse sections were made spanning the length of the humeri using a low-speed wafering blade (Phoenix 4000, Buehler). Sections were then fixed to plastic slides and ground and polished to a mirror finish using a series of grit papers followed by decreasing diameters (30 and 9 μ m) of colloidal diamond suspensions (Metadi, Buehler). Trabecular measurements were made on sections from the proximal humerus, between 1 and 1.5 mm distal to the proximal growth plate, while cortical measurements were made on diaphyseal sections cut from the cortical midshaft, just distal to the deltoid tuberosity, similar to the region of interest used for μ CT analysis.

Quantitative Backscattered Scanning Electron Microscopy (bSEM)

To measure global mineralization, polished specimen block faces were carbon coated to prevent surface charging (Cressington carbon coater 108carbon/A). Global mineralization measurements were performed using established techniques [31]. Briefly, a series of images were collected within each region of interest using an accelerating voltage of 25 kV at a magnification of $\times 150$, with a resulting pixel size of 0.67 by 0.62 μm (Hitachi S-3000N). Calibrations were performed prior to imaging by adjusting the brightness and contrast settings so that the grayscale values of aluminum and carbon tapes (electron microscopy sciences) were ~ 210 and ~ 45 , respectively. After collecting bone images, the standard materials were re-imaged to ensure beam stability throughout the imaging session. Any grayscale fluctuation of >2 units measured in the carbon standard was considered unstable and the specimen in question was re-imaged following further surface preparation.

Conversion from grayscale to Z-equivalent was performed by linear interpolation by setting the atomic number of the aluminum ($Z = 13$) and carbon ($Z = 6$). The resulting series of bSEM images was compiled per specimen and a bone mineral density distribution (BMDD) [30] was derived. The resulting BMDDs were further processed via a custom MatLab script (MathWorks) designed to assess the mean mineralization (Z) and the full width at half maximum, or the mineralization heterogeneity (Z).

Assessing Osteocytic Osteolysis

Using backscatter SEM images, lacunar area measurements were made with the built-in *Particle Analyzer* in ImageJ. Peri-lacunar mineralization was assessed by determining the mean mineralization and mineralization heterogeneity within three pixels ($\sim 2 \mu\text{m}$) of the lacunar surfaces (Fig. 1).

Fourier Transform Infrared Microspectroscopy (FTIRM)

Matrix composition was measured using Fourier transform infrared microspectroscopy (FTIRM) on a tissue-age specific basis at the National Synchrotron Light Source at Brookhaven National Laboratory (beamline U2B). Spectra for each compartment were collected in a specular reflectance configuration with the synchrotron source using a Nicolet Continuum IR microscope and a MCT-A detector (Thermo Electron Corp). A total of 128 scans were collected per pixel, with a spectral range of 650–4000 cm^{-1} and a spectral resolution of 8 cm^{-1} . The aperture was set to

10 \times 10 μm for trabecular measurements and 12 \times 12 μm for cortical. An average of 26 (± 14) and 20 (± 12) regions were collected for trabecular and cortical compartments, respectively.

Background spectra were collected using a gold-coated slide. Resulting reflection spectra were transformed into equivalent absorbance spectra using standard procedures [1, 18]. Four matrix compositional parameters were obtained from the resulting spectra; mineral-to-matrix and collagen cross-link ratios, crystallinity, and the carbonate substitution. Each individual region was baseline corrected according to validated techniques [1]. The mineral-to-matrix ratio was calculated using the phosphate peak, integrated at 900–1200 cm^{-1} (baseline correction of 900–1200 cm^{-1}) and the amide I peak, integrated at 1600–1700 cm^{-1} (baseline: 1300–1800 cm^{-1}). The carbonate substitution parameter was assessed by normalizing the carbonate peak at 1414–1424 cm^{-1} (baseline: 1300–1800 cm^{-1}) by the phosphate peak. Crystallinity was measured using the stoichiometric/non-stoichiometric phosphate ratio (1037–1033 cm^{-1} /1027–1023 cm^{-1} , baseline: 900–1200 cm^{-1}), and collagen cross-linking by the 1661–1659 cm^{-1} /1691–1689 cm^{-1} ratio (baseline: 1300–1800 cm^{-1}).

Matrix compositional parameters were measured in the new tissue, defined as tissue between the two fluorochrome labels. In the cortical compartment, there were no differences between the matrix compositional parameters measured in the periosteal and endocortical compartments (paired samples t test) and, therefore, the data were grouped. Sites of intracortical remodeling, presumably due to PTH treatment [29], were excluded from analysis.

Statistical Analysis

Data were initially tested for normality using the Kolmogorov–Smirnov test. The majority of the primary outcome variables were normally distributed. Trabecular bone volume fraction (BV/TV) however, was not normally distributed and, therefore, the data for this variable were log transformed prior to statistical analysis. All primary outcome variables were analyzed using two-way analysis of variance (ANOVA) to assess the effects of treatment (vehicle vs. iPTH) and genotype (wild-type vs. SOST KO). The presence of a significant interaction term between treatment and genotype was interpreted to mean that the iPTH treatment effect was dependent upon sclerostin status (genotype). Post hoc analysis was performed using an independent samples t -test to determine which specific treatment effects were significant within genotypes and which genotype effects were significant within treatment groups.

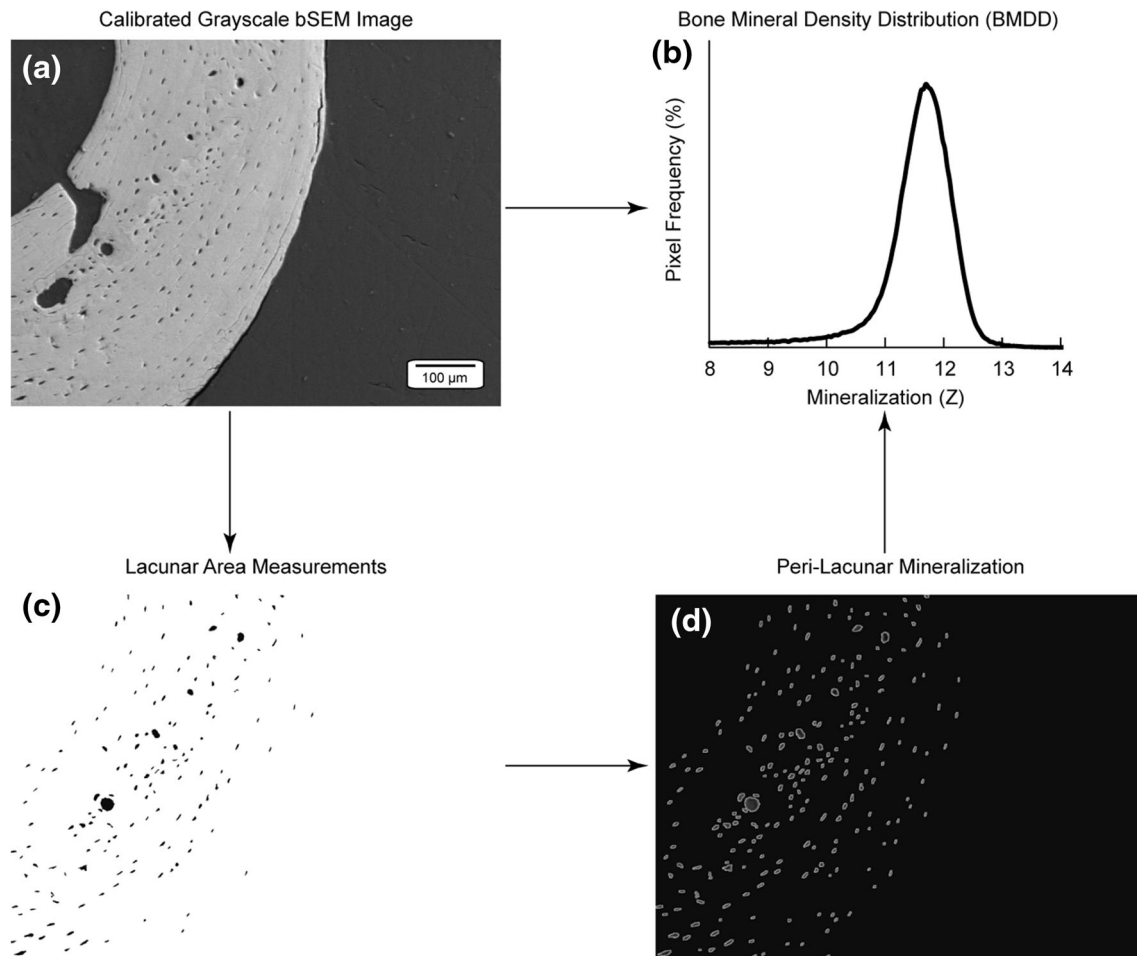


Fig. 1 bSEM imaging protocol. **a** Calibrated bSEM images are obtained across the entire cross section of the embedded humeri. **b** Histograms representing the bone mineral density distribution (BMDD) were then used to quantify the mean and the full width at

half maximum (mineralization heterogeneity). **c** Osteocytic osteolysis was evaluated by measuring the lacunar area, and by **d** deriving a second peri-lacunar BMDD to evaluate the matrix surrounding osteocytes

Table 1 Global bSEM-derived matrix mineralization parameters

	WT vehicle	WT PTH	SOST KO vehicle	SOST KO PTH	PTH effect	Genotype effect	Interaction term
Mean trabecular mineralization (Z)	11.02 (0.76)	11.20 (0.30)	10.88 (0.30)	11.03 (0.28)	0.382	0.420	0.930
Trabecular mineralization heterogeneity (Z)	1.17 (0.39)	1.90 (0.21)	1.20 (0.46)	1.51 (0.55)	0.236	0.474	0.598
Mean cortical mineralization (Z)	11.39 (0.31)	11.41 (0.22)	11.55 (0.12)	11.57 (0.65)	0.887	0.326	0.994
Cortical mineralization heterogeneity (Z)	0.95 (0.18)	1.26 (0.36)	1.43 (0.17)	1.37 (0.35)	0.310	0.024	0.154

Results

Global mineralization was assessed using backscattered scanning electron microscopy (bSEM, Table 1). Neither the global mean mineralization nor mineralization heterogeneity were affected by iPTH treatment in either the trabecular or cortical compartments. In the cortical compartment, there was a significant increase in the

mineralization heterogeneity in the SOST KO animals compared to wild-type controls (genotype effect: $p = 0.024$).

Osteocytic osteolysis was assessed by measuring the average lacunar area, lacunar density (lacunar number per area), and the peri-lacunar mineralization (mean and heterogeneity). None of the parameters measured were found to be impacted by iPTH treatment (Table 2). There

Table 2 Parameter describing osteocytic osteolysis

	WT vehicle	WT PTH	SOST KO vehicle	SOST KO PTH	PTH effect	Genotype effect	Interaction term
Trabecular lacunar area (μm^2)	26.28 (3.61)	26.52 (3.34)	25.49 (0.96)	25.11 (3.40)	0.957	0.383	0.803
Trabecular lacunar density (number/ μm^2)	630 (160)	950 (210)	820 (165)	820 (320)	0.127	0.762	0.118
Trabecular peri-lacunar mean mineralization (Z)	9.99 (0.49)	10.11 (0.22)	10.04 (0.29)	10.08 (0.14)	0.512	0.923	0.744
Trabecular peri-lacunar mineralization heterogeneity (Z)	3.25 (1.00)	3.45 (0.44)	2.98 (0.33)	3.42 (0.35)	0.211	0.543	0.634
Cortical lacunar area (μm^2)	26.74 (4.44)	26.87 (3.18)	23.88 (2.66)	24.07 (3.61)	0.918	0.081	0.986
Cortical lacunar density (number/ μm^2)	730 (420)	810 (170)	750 (90)	640 (200)	0.934	0.356	0.288
Cortical peri-lacunar mean mineralization (Z)	10.14 (0.21)	10.50 (0.31)	10.77 (0.13)	10.55 (0.80)	0.706	0.086	0.136
Cortical peri-lacunar mineralization heterogeneity (Z)	3.54 (0.39)*	2.93 (0.61)	2.72 (0.50)*	3.50 (0.50)	0.707	0.575	0.005

* Indicates post hoc significance ($p < 0.05$), independent t test

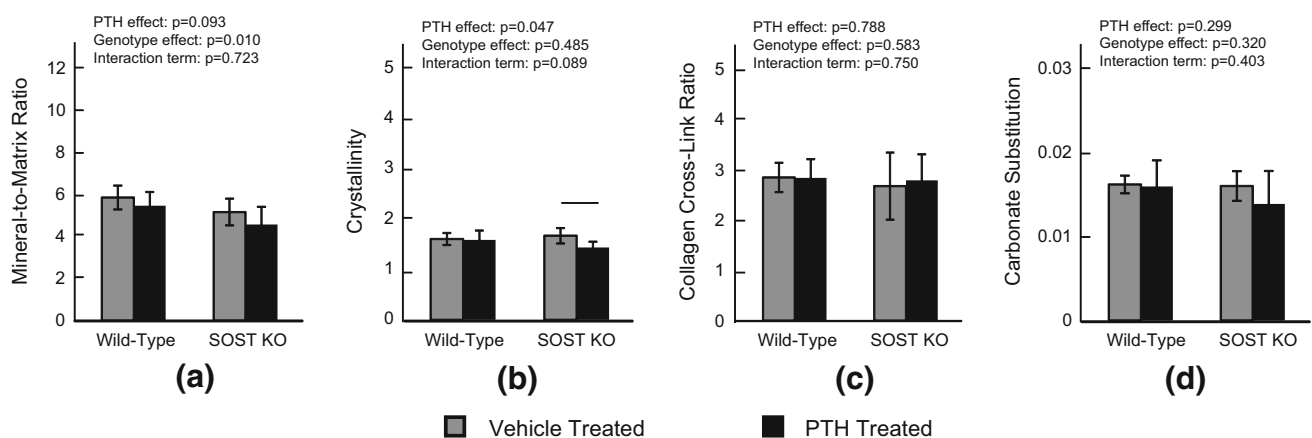


Fig. 2 Trabecular matrix composition derived using Fourier transform infrared microspectroscopy (FTIRM). Matrix compositional parameters measured include **a** mineral-to-matrix ratio, **b** crystallinity, **c** collagen cross-link ratio, and **d** carbonate substitution. Measurements were made during the 6-week treatment period. The results are

presented as the means with *error bars* showing the standard deviation. Results from the two-way ANOVA are presented in the legends. Significant post hoc tests are indicated with *horizontal bars* for specific treatment effects in animals of the same genotype ($p < 0.05$)

were no genotype effects, but there was a significant interaction term for peri-lacunar mineralization heterogeneity in the cortical compartment ($p = 0.005$) due to a non-significant reduction in mineralization heterogeneity following iPTH treatment in the wild-type animals and a significant increase in the SOST KO mice ($p = 0.014$, t test).

Matrix compositional parameters were measured within tissue formed during the 6 week treatment period. In the trabecular compartment, iPTH treatment led to decreased trabecular crystallinity (treatment effect: $p = 0.047$, Fig. 2) and marginally reduced mineral-to-matrix ratio (treatment effect: $p = 0.093$), but did not impact the other matrix compositional parameters. The mineral-to-matrix ratio was significantly reduced in the SOST KO animals compared to WT animals (genotype effect: $p = 0.010$), while no other parameters were impacted by SOST deficiency. In the

cortical compartment, iPTH treatment significantly reduced the crystallinity ($p = 0.002$, Fig. 3) and significantly increased the collagen cross-link ratio ($p = 0.028$). SOST KO animals had significantly reduced mineral-to-matrix ratio compared to their WT controls ($p = 0.016$). Carbonate substitution was not impacted by either genotype or treatment. There were no significant interactions for the matrix parameters in either compartment.

iPTH treatment increased BV/TV for both wild-type and SOST KO animals (treatment effect: $p < 0.001$, Fig. 4), and this effect was greater in the SOST KO animals than the WT animals (interaction term, $p = 0.003$). PTH treatment increased cortical area in both wild-type and SOST KO animals ($p < 0.001$). Unlike the trabecular BV/TV, there was no significant interaction for cortical area. In both compartments, SOST KO animals had greater bone mass than wild-type controls ($p < 0.001$).

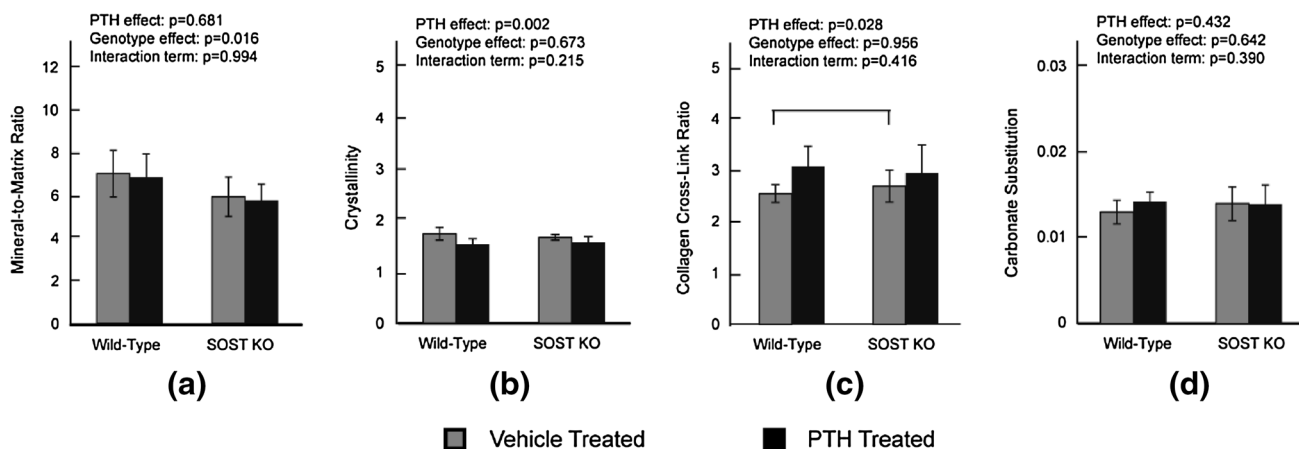
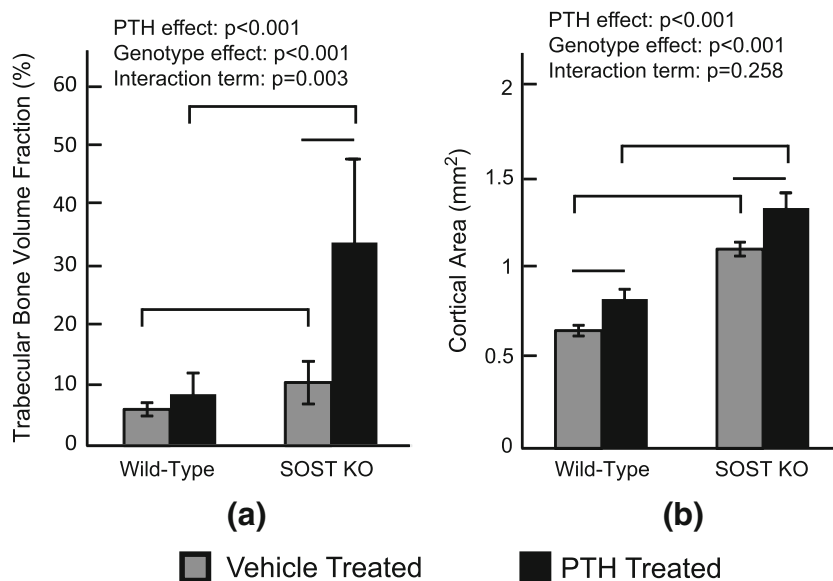


Fig. 3 Cortical matrix composition derived using Fourier transform infrared microspectroscopy (FTIRM). Matrix compositional parameters measured include **a** mineral-to-matrix ratio, **b** crystallinity, **c** collagen cross-link ratio, and **d** carbonate substitution. Measurements were made during the 6-week treatment period. The results are

presented as the means with *error bars* showing the standard deviation. Results from the two-way ANOVA are presented in the legends. Significant post hoc tests are indicated with *brackets* for specific genotype effects of similarly treated animals ($p < 0.05$)

Fig. 4 a Trabecular bone volume fraction measured in the proximal humerus and **b** cortical area measured in the humeral diaphysis. The results are presented as the means with *error bars* showing the standard deviation. Results from the two-way ANOVA are presented in the legends. Significant post hoc tests are indicated with *horizontal bars* for specific treatment effects in animals of the same genotype while *brackets* indicate specific genotype effects of similarly treated animals ($p < 0.05$)



Discussion

Sclerostin and parathyroid hormones are strong negative and positive regulators, respectively, of bone formation; yet their roles in the process of bone matrix maturation are still emerging. In the current study, we evaluated bone matrix formed in wild-type and SOST KO animals during iPTH treatment. iPTH treatment resulted in significantly increased trabecular and cortical bone mass, reduced mineral crystallinity in trabecular bone and increased collagen cross-linking in cortical bone. SOST deficiency resulted in significantly increased trabecular and cortical bone mass, and reduced mineral-to-matrix ratio in both trabecular and cortical compartments. While the magnitude

of the PTH-induced bone mass increase in trabecular bone was dependent upon sclerostin status, the matrix composition differences induced by iPTH treatment were not dependent on sclerostin status.

Bone mineralization is a dynamic process and newly formed tissues generally take time to reach mineralization maturity. Therefore, the global mineralization tends to decrease with increased bone formation rates due to the accumulation of new and relatively young tissue [30]. iPTH is known to substantially increase the bone formation rate and yet in this study and others, the global mean mineralization reduction tends to be non-significant [6, 12, 19, 20]. Although in several of these studies the mineralization heterogeneity is shown to increase in humans

following iPTH treatment [19, 20], we did not note any differences in the current study, which may be due to species differences in the inherent mineralization rate. The most consistent treatment effect was found in the crystallinity parameter, which was significantly reduced in both the trabecular and cortical tissue formed during treatment. This finding is consistent with a decreased crystallinity noted previously in primates [26] and humans [27] following iPTH treatment, which has been attributed to the formation of relatively immature tissue.

Sclerostin is a potent inhibitor of bone formation and recently it was shown to inhibit osteoblastic mineralization *in vivo* [2, 22]. Our results show a reduction in the mineral-to-matrix ratio in SOST KO animals compared to their wild-type controls, which is consistent with previous characterization of SOST deficient mice and human biopsies from patients with sclerostin mutations [9]. It is likely that this is due to the dramatically elevated bone formation rates noted in SOST KO animals [16, 29]. It is interesting that the local FTIRM measurements found reduced mineral-to-matrix due to the SOST deficiency, but the global bSEM mineralization measurements did not show any evidence of depressed mineralization. This seeming discrepancy may suggest that the reduced mineralization is transient; although Hassler et al. [9] noted that the reduced mineral-to-matrix ratio persists into tissue-ages of at least 65 days. Further, experiments are necessary to determine whether the maturation process is permanently impaired by SOST deficiency or whether there is a new peak tissue maturity level when sclerostin is absent. Additionally, it is interesting that these same effects were not noted in animals treated with sclerostin antibody [31], but this may be due to currently unrecognized matrix differences between protein suppression and genetic mutations.

Another possible explanation for the discrepancy between local FTIRM and global bSEM mineralization measurements in the SOST KO animals is an increase in the osteocytic lacunae size or density, a process termed osteocytic osteolysis, as the FTIRM measurements were performed at a considerably lower spatial resolution than was bSEM (>100 vs. $<1 \mu\text{m}^2$). Since it was possible that PTH treatment or sclerostin suppression could affect osteocytic osteolysis and, therefore, confound the global mineralization or FTIR measurements, we included analysis of the average lacunar area and the peri-lacunar mineralization. Previous studies have reported increased lacunar size following treatment with superphysiological doses of PTH [15, 32] and in biopsies from patients with hyperparathyroidism [21]. In the current study, animals were treated with intermittent PTH, which did not alter any of the osteocytic osteolysis parameters, suggesting that PTH concentration must be consistently elevated to induce a catabolic phenotype in osteocytes. Similar to

PTH, increasing the SOST concentration, by providing recombinant sclerostin to cultured osteocytes [13] or by transgenic manipulation in mice [13] has been shown to induce osteoclast-like phenotypes in osteocytes. In the current study, SOST deficiency was not found to affect osteocytic osteolysis. Therefore, although osteocytic osteolysis may work through a sclerostin-dependent mechanism, it appears that under normal bone development, sclerostin is not necessary for peri-lacunar matrix maturation.

Emerging evidence has suggested that the anabolic responses associated with PTH treatment and sclerostin suppression are not independent. Indeed, treatment with PTH has been shown to cause substantial sclerostin suppression [3, 11] and the anabolic effects of PTH appear to depend on sclerostin status [14, 29]. Two published studies have investigated the skeletal response to PTH in animals with genetic sclerostin modifications. Kramer et al. [14] found that bone formation was attenuated in both sclerostin knockout and sclerostin overexpressing mice. On the other hand, we have reported a compartment-specific response—cortical bone mass gains were offset by an increased resorptive response to PTH, while the anabolic effects of PTH in trabecular bone appeared to be largest in the sclerostin knockout mice [29]. Tissues from the current study were derived from our previous study, and therefore, it isn't surprising that the current results show an increased anabolic response to iPTH in the trabecular compartment of the sclerostin deficient animals. In the cortical compartment, the sclerostin knockout animals seemed to build bone similarly to wild-types in response to iPTH, although we did not measure bone resorption or cortical porosity in this experiment.

Despite the interaction between PTH and SOST from previous studies and those found in the bone volume data in the current study, the matrix composition differences between vehicle and PTH-treated mice were not dependent upon sclerostin status. Specifically, the reduced crystallinity following iPTH treatment occurred independent of the sclerostin deficiency, while the reduced mineral-to-matrix ratio in the SOST KO animals was present in both vehicle and PTH-treated cohorts. Therefore, the assessed PTH effects on bone matrix composition were independent of SOST status in the present study.

The current study was limited by a relatively small sample size. Despite this limitation, the majority of the primary endpoints were normally distributed and several parameters showed significant genotype and/or PTH treatment differences. The combined use of techniques presented in the present study and future materials characterization will allow for further understanding of the role of these two proteins in the bone matrix maturation process.

Conclusion

The current study evaluated matrix composition following intermittent PTH treatment in wild-type and SOST KO mice. iPTH treatment-reduced crystallinity, while SOST deficiency led to decreased mineral-to-matrix ratio in both trabecular and cortical compartments. Similarly, iPTH treatment and SOST deficiency increased bone mass in both compartments. The iPTH-induced changes in bone mass were dependent upon sclerostin status in the trabecular compartment, but not in the cortical compartment. In contrast, iPTH-induced changes in matrix composition were sclerostin-independent in both trabecular and cortical compartments.

Acknowledgments The authors acknowledge Randy Smith at the National Synchrotron Light Source of Brookhaven National Laboratory for his help in the use of the FTIRM. The National Synchrotron Light Source is supported by the U.S. Department of Energy under Contract No. DE-AC02-98CH10886. μ CT scanning was performed at the Rush University Medical Center MicroCT/Histology Core.

Compliance with Ethical Standards

Conflict of Interest Ryan D. Ross, Maleeha Mashiatulla, Alexander G. Robling, Lisa M. Miller, D. Rick Sumner declare that they have no conflict of interest.

Human and Animal Rights and Informed Consent This article does not contain studies with human participants performed by any of the authors. All procedures performed in studies involving animals were in accordance with the ethical standards of the institution at which the studies were performed.

Funding This work was supported by NIH Grant AR53237 and VA Grant BX001478 (to AGR).

References

1. Acerbo AS, Carr GL, Judex S, Miller LM (2012) Imaging the material properties of bone specimens using reflection-based infrared microspectroscopy. *Anal Chem* 84:3607–3613
2. Atkins GJ, Rowe PS, Lim HP, Welldon KJ, Ormsby R, Wijenayaka AR, Zelenchuk L, Evdokiou A, Findlay DM (2011) Sclerostin is a locally acting regulator of late-osteoblast/pre-osteocyte differentiation and regulates mineralization through a MEPE-ASARM-dependent mechanism. *J Bone Miner Res* 26:1425–1436
3. Bellido T (2006) Downregulation of SOST/sclerostin by PTH: a novel mechanism of hormonal control of bone formation mediated by osteocytes. *J Musculoskelet Neuronal Interact* 6:358–359
4. Bouxsein ML, Boyd SK, Christiansen BA, Guldberg RE, Jepsen KJ, Muller R (2010) Guidelines for assessment of bone microstructure in rodents using micro-computed tomography. *J Bone Miner Res* 25:1468–1486
5. Burr DB (2002) Bone material properties and mineral matrix contributions to fracture risk or age in women and men. *J Musculoskelet Neuronal Interact* 2:201–204
6. Cheng Z, Yao W, Zimmermann EA, Busse C, Ritchie RO, Lane NE (2009) Prolonged treatments with antiresorptive agents and PTH have different effects on bone strength and the degree of mineralization in old estrogen-deficient osteoporotic rats. *J Bone Miner Res* 24:209–220
7. de Paula FJ, Rosen CJ (2010) Back to the future: revisiting parathyroid hormone and calcitonin control of bone remodeling. *Horm Metab Res* 42:299–306
8. Felsenberg D, Boonen S (2005) The bone quality framework: determinants of bone strength and their interrelationships, and implications for osteoporosis management. *Clin Ther* 27:1–11
9. Hassler N, Roschger A, Gamsjaeger S, Kramer I, Lueger S, van Lierop A, Roschger P, Klaushofer K, Paschalis EP, Kneissel M, Papapoulos S (2014) Sclerostin deficiency is linked to altered bone composition. *J Bone Miner Res* 29:2144–2151
10. Hodsman AB, Bauer DC, Dempster DW, Dian L, Hanley DA, Harris ST, Kendler DL, McClung MR, Miller PD, Olszynski WP, Orwoll E, Yuen CK (2005) Parathyroid hormone and teriparatide for the treatment of osteoporosis: a review of the evidence and suggested guidelines for its use. *Endocr Rev* 26:688–703
11. Keller H, Kneissel M (2005) SOST is a target gene for PTH in bone. *Bone* 37:148–158
12. Kneissel M, Boyde A, Gasser JA (2001) Bone tissue and its mineralization in aged estrogen-depleted rats after long-term intermittent treatment with parathyroid hormone (PTH) analog SDZ PTS 893 or human PTH (1–34). *Bone* 28:237–250
13. Kogawa M, Wijenayaka AR, Ormsby R, Thomas GP, Anderson PH, Bonewald LF, Findlay DM, Atkins GJ (2013) Sclerostin regulates release of bone mineral by osteocytes by induction of carbonic anhydrase 2. *J Bone Miner Res* 28:2436–2448
14. Kramer I, Loots GG, Studer A, Keller H, Kneissel M (2010) Parathyroid hormone (PTH) induced bone gain is blunted in SOST overexpressing and deficient mice. *J Bone Miner Res* 25:178–189
15. Krempien B, Friedrich E, Ritz E (1978) Effect of PTH on osteocyte ultrastructure. *Adv Exp Med Biol* 103:437–450
16. Li X, Ominsky M, Niu Q, Sun N, Daugherty B, D'Agostin D, Kurahara C, Gao Y, Cao J, Gong J, Paszty C, Ke HZ, Simonet WS (2008) Targeted deletion of the sclerostin gene in mice results in increased bone formation and bone strength. *J Bone Miner Res* 23:860–869
17. Lombardi G, Di Somma C, Rubino M, Faggiano A, Vuolo L, Guerra E, Contaldi P, Savastano S, Colao A (2011) The roles of parathyroid hormone in bone remodeling: prospects for novel therapeutics. *J Endocrinol Invest* 34:18–22
18. Miller LM, Little W, Schirmer A, Sheik F, Busa B, Judex S (2007) Accretion of bone quantity and quality in the developing mouse skeleton. *J Bone Miner Res* 22:1037–1045
19. Misof BM, Paschalis EP, Blouin S, Fratzl-Zelman N, Klaushofer K, Roschger P (2010) Effects of 1 year of daily teriparatide treatment on iliac bone mineralization density distribution (BMDD) in postmenopausal osteoporotic women previously treated with alendronate or risedronate. *J Bone Miner Res* 25:2297–2303
20. Misof BM, Roschger P, Cosman F, Kurland ES, Tesch W, Messmer P, Dempster DW, Nieves J, Shane E, Fratzl P, Klaushofer K, Bilezikian J, Lindsay R (2003) Effects of intermittent parathyroid hormone administration on bone mineralization density in iliac crest biopsies from patients with osteoporosis: a paired study before and after treatment. *J Clin Endocrinol Metab* 88:1150–1156
21. Mosekilde L, Melsen F (1978) A tetracycline-based histomorphometric evaluation of bone resorption and bone turnover in hyperthyroidism and hyperparathyroidism. *Acta Med Scand* 204:97–102
22. Ota K, Quint P, Ruan M, Pederson L, Westendorf JJ, Khosla S, Oursler MJ (2013) Sclerostin is expressed in osteoclasts from aged mice and reduces osteoclast-mediated stimulation of mineralization. *J Cell Biochem* 114:1901–1907

23. Padhi D, Allison M, Kivitz AJ, Gutierrez MJ, Stouch B, Wang C, Jang G (2013) Multiple doses of sclerostin antibody romosozumab in healthy men and postmenopausal women with low bone mass: A randomized, double-blind, placebo-controlled study. *J Clin Pharmacol* 54:168–178
24. Padhi D, Jang G, Stouch B, Fang L, Posvar E (2011) Single-dose, placebo-controlled, randomized study of AMG 785, a sclerostin monoclonal antibody. *J Bone Miner Res* 26:19–26
25. Padhi D, Stouch B, Jang G, Fang L, Darling M, Glise H, Robinson M, Harris S, Posvar E (2007) Anti-sclerostin antibody increases markers of bone formation in healthy postmenopausal women. *J Bone Miner Res* 22:S37
26. Paschalis EP, Burr DB, Mendelsohn R, Hock JM, Boskey AL (2003) Bone mineral and collagen quality in humeri of ovariectomized cynomolgus monkeys given rhPTH (1-34) for 18 months. *J Bone Miner Res* 18:769–775
27. Paschalis EP, Glass EV, Donley DW, Eriksen EF (2005) Bone mineral and collagen quality in iliac crest biopsies of patients given teriparatide: new results from the fracture prevention trial. *J Clin Endocrinol Metab* 90:4644–4649
28. Recker R, Benson C, Matsumoto T, Bolognese M, Robins D, Alam J, Chiang AY, Hu L, Krege JH, Sowa H, Mitlak B, Myers S (2014) A randomized, double-blind phase 2 clinical trial of blosozumab, a sclerostin antibody, in postmenopausal women with low bone mineral density. *J Bone Miner Res* 30:216–224
29. Robling AG, Kedlaya R, Ellis SN, Childress PJ, Bidwell JP, Bellido T, Turner CH (2011) Anabolic and catabolic regimens of human parathyroid hormone 1-34 elicit bone- and envelope-specific attenuation of skeletal effects in Sost-deficient mice. *Endocrinology* 152:2963–2975
30. Roschger P, Paschalis EP, Fratzl P, Klaushofer K (2008) Bone mineralization density distribution in health and disease. *Bone* 42:456–466
31. Ross RD, Edwards LH, Acerbo AS, Ominsky MS, Viridi AS, Sena K, Miller LM, Sumner DR (2014) Bone matrix quality following sclerostin antibody treatment. *J Bone Miner Res* 29:1597–1607
32. Tazawa K, Hoshi K, Kawamoto S, Tanaka M, Ejiri S, Ozawa H (2004) Osteocytic osteolysis observed in rats to which parathyroid hormone was continuously administered. *J Bone Miner Metab* 22:524–529
33. van Bezooijen RL, ten Dijke P, Papapoulos SE, Lowik CW (2005) SOST/sclerostin, an osteocyte-derived negative regulator of bone formation. *Cytokine Growth Factor Rev* 16:319–327